Title:
Precision Targeting with EZH2 and HDAC Inhibitors in Epigenetically Dysregulated Lymphomas

Authors:
Jennifer K. Lue[1]*, Sathyen A. Prabhu[1]*, Yuxuan Liu[1], Yulissa Gonzalez[1], Akanksha Verma[2], Prabhjot S. Mundi[3], Nebiyu Abshiru[4], Jeannie M. Camarillo[4], Swasti Mehta[1], Emily I. Chen[5], Changhong Qiao[6], Renu Nandakumar[6], Serge Cremers[6], Neil L. Kelleher[4], Olivier Elemento[2], and Jennifer E. Amengual[1]
*equal contribution

Affiliations:
1. Center for Lymphoid Malignancies, Department of Medicine, Columbia University Medical Center, NY, NY; 2. Caryl and Israel Englander Institute for Precision Medicine, HRH Prince Alwaleed Bin Talal Bin Abdulaziz Alsaud Institute for Computational Biomedicine, Weill Cornell Medical College, NY, NY; 3. Department of Medicine, Columbia University Medical Center, NY, NY; 4. Departments of Chemistry and Molecular Biosciences and the Feinberg School of Medicine, Northwestern University; 5. Department of Pharmacology and the Herbert Irving Comprehensive Cancer Center Proteomics Shared Resource, Columbia University Medical Center, NY, NY. 6. Clinical Translational Research Center, Laboratory of Analytical Pharmacology, Columbia University Medical Center – College of Physicians and Surgeons, New York, N.Y.

Running Title:
Precision Targeting with EZH2 and HDAC Inhibitors

Key Words:
Epigenetics, Lymphoma, EZH2 inhibitors, methylation, acetylation

Corresponding Author:
Jennifer E. Amengual, MD
51 W 51st Street, Suite 200
New York, NY 10019
jea2149@columbia.edu
Phone: 212-326-5720
Fax: 212-326-5725

Text Word Count: 4810
Abstract Word Count: 249
Figures: 6
Supplementary Figures: 7
References: 50

ABBREVIATIONS LIST

EZH2: enhancer of zeste homolog 2; HDAC: histone deacetylase; PRC2: polycomb repressive complex 2; GC: germinal center; DLBCL: diffuse large B-cell lymphoma; RbAP 46/48: Retinoblastoma associated proteins 46/48; DNMT: DNA methyltransferase; HAT: histone acetyltransferase; EP300: E1A Binding Protein P300; CREBBP: CREB Binding Protein; metaVIPER: meta- Virtual Inference of Protein-activity by Enriched Regulon analysis

CONFLICT OF INTEREST

JEA has received honorarium from Janssen and receives research funding from Appia Pharmaceuticals. All other authors declare no potential conflicts of interest.

ABSTRACT

Purpose: Both gain-of-function EZH2 mutations and inactivating histone acetyltransferases mutations, such as CREBBP and EP300, have been implicated in the pathogenesis of germinal center (GC) derived lymphomas. We hypothesized that direct inhibition of EZH2 and HDAC would be synergistic in GC-derived lymphomas.

Experimental Design: Lymphoma cell lines (n=21) were exposed to GSK126, an EZH2 inhibitor, and romidepsin, a pan-HDAC inhibitor. Synergy was assessed by Excess over Bliss. Western blot, mass spectrometry and co-immunopreciptiation were performed. A SU-DHL-10 xenograft model was utilized to validate *in vitro* findings. Pre-treatment RNA-sequencing of cell lines was performed. MetaVIPER analysis was used to infer protein activity.

Results: Exposure to GSK126 and romidepsin demonstrated potent synergy in lymphoma cell lines with EZH2 dysregulation. Combination of romidepsin with other EZH2 inhibitors also demonstrated synergy suggesting a class effect of EZH2 inhibition with romidepsin. Dual inhibition of EZH2 and HDAC led to modulation of acetylation and methylation of H3K27. The synergistic effects of the combination was due to disruption of the PRC2 complex secondary to acetylation of RbAP 46/48. A common basal gene signature was shared among synergistic lymphoma cell lines and were characterized by upregulation in chromatin remodeling genes and transcriptional regulators. This finding was supported by metaVIPER analysis which also revealed that HDAC 1/2 and DNMT were associated with EZH2 activation.

Conclusions: Inhibition of EZH2 and HDAC is synergistic and leads to the dissociation of PRC2 complex. Our findings support the clinical translation of the combination of EZH2 and HDAC inhibition in EZH2 dysregulated lymphomas.

STATEMENT OF TRANSLATIONAL RELEVANCE

Given the prevalence of EZH2 mutations and HAT mutations in germinal center diffuse large B-cell lymphoma, the rational combination of EZH2 inhibition and HDAC inhibition was explored. Using a panel of 21 lymphoma cell lines, we demonstrate that exposure to dual inhibition of EZH2 and HDACs was synergistic in EZH2 dysregulated lymphomas. The synergistic effects of EZH2 and HDAC inhibition may be attributed to the disassembly of the PRC2 complex. In a mouse xenograft model of SU-DHL-10, the combination led to tumor growth delay and an improvement in overall survival. A basal common genetic signature amongst synergistic cell lines was identified using GSEA and metaVIPER analysis and correlates with therapeutic response. The novel combination of dual EZH2 and HDAC inhibition may serve as a future precision medicine therapeutic platform. A clinical trial to further explore this combination is in development.

INTRODUCTION

Enhancer of zeste homolog 2 (EZH2) is critical in the germinal center (GC) reaction and serves as the catalytic subunit of the Polycomb Repression Complex 2 (PRC2), inducing tri-methylation of histone 3 lysine 27 (H3K27me3), a marker of transcriptional repression[1]. During the GC reaction, the PRC2 complex recruits histone deacetyltransferase (HDAC) 1/2 and DNA methyltransferases (DNMT) to further inhibit transcription[2,3].

Disturbances in epigenetic pathways have been implicated in lymphomagenesis. Aberrancy of histone methyltransferases, such as EZH2, have been associated with the development of GC-derived lymphomas, including diffuse large B cell lymphoma (DLBCL) and follicular lymphoma (FL)[4,5]. Activating mutations in EZH2 have been implicated in 22% of GC-DLBCL and 7-12% of FL[4,5]. EZH2 dysregulation has been implicated in other lymphoma subtypes, including overexpression in some subtypes of T-cell lymphoma (TCL)[6-9]. Given the prevalence of EZH2 dysregulation in several malignancies, EZH2 inhibitors have been developed, and demonstrate superior efficacy in mutated EZH2 GC-derived lymphoma cell lines compared to wildtype EZH2 cell lines[10-12]. The preclinical activity of the EZH2 inhibitors in B-cell lymphomas has been replicated in the clinic by tazemetostat, a first-in-class EZH2 inhibitor, which demonstrated an overall response rate of 38% in a phase I clinical trial[13]. Notably, clinical responses were achieved irrespective of EZH2 mutational status.

Also contributing to GC-lymphomagenesis is the haploinsufficiency of histone acetyltransferases (HATs). HATs control the addition of acetyl groups on histones in order to promote an open chromatin state, allowing for transcription. Mutations leading to loss of function of HATs, specifically EP300 and CREBBP, are found in 39% of GC-DLBCLs and 41% of FLs[14], and the presence of these mutations has been reported to be associated with HDAC inhibitor sensitivity[15]. Vorinostat, an HDAC inhibitor, was the first epigenetic drug to gain FDA approval in patients with relapsed/refractory TCL. Two other HDAC inhibitors have gained approval for the

treatment of TCL, while panobinostat has been approved for the treatment of multiple myeloma. However, despite the robust link between epigenetic dysregulation in several malignancies, few diseases have demonstrated clinical benefit with single agent epigenetic targeting therapy, including GC-derived B-cell lymphomas.

Our group and others have established a proof-of -principle for selective targeting of epigenetic modifiers in DLBCL. The combination of niacinamide, a sirtuin inhibitor, and pan-HDAC inhibitors, including romidepsin, are synergistic in GC-DLBCL[16]. A phase I clinical study utilizing vorinostat and niacinamide in relapsed/refractory lymphoma demonstrated an ORR of 24% suggesting a potential role for combination epigenetic therapy in B-cell lymphomas. The combination of panobinostat and decitabine, a DNMT inhibitor, was found to be more synergistic in GC-DLBCL compared to Activated B-Cell (ABC) DLBCL cell lines leading to a unique differential expression of various genes including SMAD1 and DNMT3A[17]. Although single agent epigenetic therapy has been disappointing in DLBCL, the aforementioned data suggests that using a platform based on a combination of epigenetic targeted agents may be a potential therapeutic method for the treatment of GC-DLBCL.

Given the frequent dysfunction of EZH2 as well as HATs in GC-derived B-cell lymphomas, we hypothesized that the rational combination of EZH2 and HDAC inhibitors would be synergistic by modulating both acetylation and methylation states, in turn, triggering apoptosis. Simultaneous mutations in EZH2 and CREBBP occur in 26/1343 primary DLBCL samples (adjusted p-value < 0.001), while co-occurrence of mutations of EZH2 and EP300 are not significant (7/1343)[18,19]. Herein, we demonstrate that GSK126, an EZH2 inhibitor, and romidepsin, a pan-HDAC inhibitor, are synergistic by disrupting the PRC2 complex, leading to modulation of histone acetylation and methylation. Sensitivity to the combination was associated with a specific gene expression signature.

MATERIAL and METHODS

Cell Lines and Culture

OCI-LY1, SU-DHL-2, SU-DHL-6, Pfeiffer, Farage, Toledo, Riva, HBL-1, Jeko-1, Z-138, H9, and HH were obtained from ATCC. OCI-LY7, OCI-LY10, SU-DHL-10 and OCI-LY3 were obtained from DSMZ. PF382, and P12 were gifts from the laboratory of Adolfo Fernando. TLOM-1 and MT-1 was obtained from Kyoto University; and MT-2 was obtained from Memorial Sloan Kettering Cancer Center. All cell lines were authenticated and screened for mycoplasma using the ATCC/Promega STR Authentication Testing Kit and Lonza MycoAlert, obtained between 2008-2016 and revived after 2 weeks. Experiments were performed between 2015-2018.

EZH2 PCR

Genomic DNA from 21 lymphoma cell lines were extracted with cell culture DNA mini Kit (Qiagen) and measured by NanoDrop 3300. PCR was performed by following the manufacturer's instructions. Genomic DNA was amplified by PCR with AmpliTaq Gold DNA Polymerase, PE Buffer II and $MgCl_2$ (Applied Biosystems) using primers designed as follows: EZH2 Y641 forward, 5'-CAGGTCTGAGGATTTACAGTGATAG-3'; EZH2 Y641 reverse, GCAGAAGTCCAGGCTGAAA-3'; EZH2 A677 forward 5'- GGCAAACCCTGAAGAACTGTA -3'; EZH2 A677 reverse 5'-GTCCATCATCACAGGACTGAAA-3'. PCR products were run on an agarose gel, purified using QIAquick PCR purification kit (28104) and sent for sequencing (Genewiz).

Cell Viability Assays

Cells were counted and re-suspended based on their optimal density for log-phase growth. Cell viability assays were performed as previously described[17]. Cells were exposed to romidepsin (Selleckchem), ACY957 (Acetylon), GSK126 (Selleckchem), EPZ011989 (Epizyme), and CPI-1205 (Selleckchem). Synergy was assessed by excess over bliss (EOB)[20,21]. Sensitivity to GSK126 and romidepsin as determined by mean IC_{50}

was correlated with EZH2 mutation/overexpression and HAT mutations, respectively, using Prism GraphPad's student paired t-test. Experiments were performed in triplicate and repeated at least twice.

Flow Cytometry

Flow cytometry analysis was performed using FITC Annexin V Apoptosis Detection Kit with PI (Biolegend #640194) as previously described[16]. Experiments were performed at least three times.

Co-Immunoprecipitation

Immunoprecipitation was performed using the Pierce™ Co-Immunoprecipitation Kit (#26149). Columns were prepared with 20-40 ug of antibody. Whole Protein lysate was incubated with antibody. Flow through was collected and column was washed and eluted. Antibodies used were: anti-EZH2 (Cell Signaling Technology), anti-SUZ12 (Cell Signaling Technology), anti-RbAP 46/48 (Cell Signaling Technology), anti-EED (Millipore), anti-HDAC2 (Cell Signaling Technology), anti-DNMT3L (Novus Biologicals). Experiments were performed at least three times.

Western Blotting

Western blotting was performed as previously described[16]. Antibodies used as above. Experiments were performed at least three times.

Mass Spectrometry for acetylation of PRC2 Complex

Immunoprecipitation was performed using Thermo Scientific™ Pierce™ MS-Compatible Magnetic IP Kit. Protein was incubated with EZH2 or acetylated-lysine antibody. Antibody bound proteins were eluted and run into SDS-PAGE. The excised gel lane pieces were reduced, alkylated, and digested in Trypsin Gold (Promega) digestion buffer (Thermo Fischer Scientific). Peptides were extracted with 70% acetonitrile (Thermo Fischer Scientific). The concentrated peptide mix was reconstituted in a solution of 2 % ACN, 2 % formic acid for MS

analysis. Peptides were eluted from the column using a Dionex Ultimate 3000 Nano LC system. Using Thermo Fusion Tribrid mass spectrometer (Thermo Scientific), eluted peptides were electrosprayed. Mass spectrometer-scanning functions and HPLC gradients were controlled by the Xcalibur data system (Thermo Fischer). Experiments were performed at least twice.

Database Search and Interpretation of MS/MS Data

Tandem mass spectra from raw files were searched against uniprot_human_170129.fasta data base using the Proteome Discoverer 2.1 (Thermo Fischer). The mouse protein database was downloaded as FASTA-formatted sequences from Uniprot protein database (January 2017). The peptide mass search tolerance was 10ppm with a required minimum sequence length of 7 amino acids. To calculate confidence levels and false positive rates (FDR), Proteome Discoverer generates a decoy database and performs the search against this concatenated database (non-decoy + decoy). Scaffold (Proteome Software, Inc) was used to visualize and filter to <1% FDR. Spectral counts were used for estimation of relative protein abundance.

HDAC shRNA

Human HDAC2 shRNA plasmids were purchased from Origene (#TG312495). HEK293 cells were plated in OPTI-MEM containing shRNA or scramble using Lipofectamine 3000 (Cat#L3000075). Cells were selected with puromycin, periodically analyzed by flow cytometry and fluorescent microscopy to monitor GFP levels until a stable cell line had been generated.

MS analysis and data handling for H3K27 acetylation and methylation

Histone extraction, derivatization, and tryptic digestion were adapted from previous works[22,23]. Peptides were resuspended in 0.1% TFA for LC-MS/MS analysis.

Multiple reaction monitoring was performed on a triple quadrupole (QqQ) mass spectrometer (Thermo Fisher Scientific TSQ Quantiva) directly coupled with UltiMate 3000 Dionex nano-LC system. The following QqQ settings were used: collision gas pressure of 1.5 mTorr; Q1 peak width of 0.7 (FWHM); cycle time of 2s; skimmer offset of 10 V; electrospray voltage of 2.5 kV. Modified and unmodified histone peptides monitored in the assay were selected based on previous reports[23]. Raw MS files were imported and analyzed in Skyline software with Savitzky-Golay smoothing[24]. Automatic peak assignments from Skyline were manually confirmed. Peptide peak areas from Skyline were used to determine the relative abundance of each histone modification. The relative abundances were determined based on the mean of three technical replicates with error bars representing the standard deviation. Experiments were performed at least twice.

In Vivo Studies

Animals were maintained in accordance with an Institutional Animal Care and Use Committee approved protocol (AC-AAAR9404). SU-DHL-10 (1×10^7) was suspended in 50% Matrigel (BD Biosciences) and 50% PBS (Gibco) and subcutaneously injected into the flanks of 5-7-week-old beige/SCID female mice (Taconic Farms). Mice were randomly divided into 5 cohorts (n= 9-10) upon tumor volume reaching 80-100 mm^3 as follows: (i) Normal saline: days 1, 4, 8, 15, 18; (ii) GSK126: 100mg/kg days 1, 4, 8, 11, 15, 18; (iii) romidepsin: 2 mg/kg days 1, 8, 15; (iv) GSK126 and romidepsin; (v) pre-treatment with GSK126 (days 1, 4, 8, 15), and followed by romidepsin on days 8, 15, 22. Dosing was selected based on prior in vivo studies[11,25,26]. Drugs were diluted in sterile normal saline and administered via intraperitoneal route. Weight and tumor volume were evaluated 3x/week. Statistical analysis was performed using two-way ANOVA Analysis, and overall survival (OS) was estimated using the Kaplan–Meier method (GraphPad Software, Inc.)

Pharmacokinetic/Pharmacodynamics in vivo studies

Plasma samples were collected at 0.25 hour (h), 0.5 h, 2 h, 4 h, 8 h and 24 h after one-time infusion of GSK126 and romidepsin. Non-compartmental analysis was performed using Phoenix Winnonlin software (Certara) to

define the maximum plasma concentration (Cmax), the time to maximum plasma concentration (Tmax), and the area under the plasma concentration time curve from t=0 to the last data point (AUClast). Romidepsin and GSK126 were extracted by mixing 2:1 solution of serum/tissue homogenate in acetonitrile/methanol.

LC-MS/MS analysis was performed using Agilent 6410 triple quad mass spectrometer (Agilent Technologies). Data acquisition and peak integration was done using MassHunter software v 3.1. The assay performance was validated for mouse serum samples according to FDA guidelines[27]. Intra-assay precision and accuracy for romidepsin in mouse serum was 5.55% and 105.1% respectively, while the inter-assay precision was 5.1%. For GSK126, the intra-assay accuracy was 99.35% with a precision of 1.55%, whereas the inter-assay precision was 2.83%.

RNA-SEQ

RNA was purified using the RNAeasy Plus Kit (QIAGEN). RNA concentration and integrity was verified using Agilent 2100 Bioanalyzer (Agilent Technologies). Libraries were generated using Illumina's TruSeq RNA sample Prep Kit v2, following the manufacturer's protocol. 2x75 bp paired-end sequencing were performed on the HiSeq4000 sequencer. Raw RNA-Seq data was aligned to the Human reference genome (Version hg19 from UCSC) using the STAR (V 2.4.2) aligner [28]. Aligned reads were quantified against the reference annotation (hg19 from UCSC) to obtain Fragments per Kilobase per million (FPKM) and raw counts using Cufflinks(v 2.2.1) and HTseq, respectively[29,30]. Differential expression was performed on raw counts with the limma package in R[31]. Principal Component analysis (PCA) was performed on the $\log_2$ transformed FPKM expression values in R statistical software. Gene Set Enrichment Analysis (GSEA) was performed using software from Broad Institute. Genes were ranked by the t-statistic value and used to identify significantly enriched biological pathways. Differential expression was performed and expression profiles of synergistic (EOB>20) vs. non-synergistic (EOB<20) cell lines were compared.

metaVIPER Analysis

The Virtual Inference of Protein-activity by Enriched Regulon analysis (VIPER) algorithm is a computational systems biology approach to infer protein activity from gene expression profiling[32,33]. In the absence of an available cancer-type specific regulatory network, metaVIPER[34] can be effectively used to infer protein activity.

All regulatory networks used for metaVIPER analysis were reverse engineered by ARACNe[35]. Twenty four core TCGA RNA-Seq derived interactomes are publicly available in the R Bioconductor package aracne.networks[36]. After standard read alignment of RNA-Seq data by STAR to the GRCh38 reference genome build and summarization of expression quantities at the gene count level, gene expression was normalized by the Variance Stabilization Transformation, as implemented in the DESeq2 package on Bioconductor[37]. A gene expression signature was computed between each synergistic cell line versus the reference group of non-synergistic cell lines using the viperSignature function in the VIPER package, followed by application of the analytic Rank-based enrichment analysis using each of the available interactomes[38,39]. Normalized enrichment scores are integrated by Stouffer's method. Pathway analysis on the differential protein activity signature was performed using GSEA with 'Cancer Hallmark' and 'Gene Ontology' gene sets provided in the Broad MSigDB collections[40].

A machine learning classifier for predicting synergy with GSK126 and romidepsin using basal protein activity signatures was developed after first running VIPER on scaled gene expression signatures, resulting in protein activity profiles for each sample. The random forest method was applied iteratively with the addition of anywhere from 1 to 100 of the most differentially active proteins between synergistic and non-synergistic cell lines. For each split in the decision trees, the minimum of the number of proteins made available for classification of 5 was used. The random Forest algorithm was run with 1000 iterations of 3-fold cross-validation to estimate the receiver operating characteristics.

RESULTS

GSK126 and romidepsin synergize in EZH2 dysregulated lymphomas

To understand the effects of EZH2 inhibition and HDAC inhibition in cell lines with or without EZH2 dysfunction and HAT mutations, a panel of 21 lymphoma cell lines were exposed to GSK126, an EZH2 inhibitor, and romidepsin, a pan-HDAC inhibitor, as single agents. Both B-cell lymphoma and TCL were selected in order to establish a range of drug sensitivity and mutational status. EZH2 mutational status was confirmed via PCR, while EZH2 overexpression and HAT mutational status was established from literature including Cancer Cell Line Encyclopedia (CCLE, Broad Institute). The concentration : effect relationship of 21 cell lines were established over varying time exposures and increasing concentrations to determine the IC_{50} to GSK126 and romidepsin (Figure 1). Lymphoma cell lines with an activating mutation in EZH2 were more sensitive to GSK126 as compared to wildtype EZH2 ($p= 0.02$) as rank ordered by the IC_{50} at 144 hours (Figure 1 A, C). In regards to cell lines with EZH2 overexpression, there was no clear association with increased sensitivity to GSK126 as compared to wildtype ($p=0.52$). Published literature suggests that HAT mutations predict sensitivity to HDAC inhibitors[14,15]. However, only a trend towards romidepsin sensitivity and the presence of EP300 or CREBBP mutation was observed ($p=0.05$) (Figure 1 B, D).

To investigate the dual effects of EZH2 inhibition and HDAC inhibition (Figure 2A), lymphoma cell lines were simultaneously exposed to GSK126 and romidepsin over 72 hours. Low drug concentrations (IC_{20-40}) were selected in order prevent untoward toxicity that may be seen with high concentration when combined. Co-exposure to GSK126 and romidepsin demonstrated potent synergy with the highest EOB value reaching 61.7 (Figure 2B, Supplementary Fig. S1). Cell lines harboring EZH2 mutations demonstrated the highest level of synergy. Drug schedule with pre-treatment of GSK126 was evaluated but did not impact synergy (Supplementary Fig. S2A, B). Combination of romidepsin with other EZH2 inhibitors including EPZ011989 and CPI-1205 also demonstrated synergy suggesting that the combination of EZH2 inhibition and romidepsin is a class effect of EZH2 (Supplementary. Fig S3).

To confirm induction of apoptosis, 4 GC-DLBCL cell lines with different EZH2 mutational status were simultaneously treated with GSK126 and romidepsin for 24-48 hours and evaluated by flow cytometry (Figure 2C-D, Supplementary Fig. S4). A time point of prior to the maximum EOB value was selected in order to capture the events prior to complete cellular demise (24 hours for Pfeiffer; 48 hours for OCI-LY7, SU-DHL-10, SU-DHL-6). Increased apoptosis was observed with the combination as compared to single agent exposure. Apoptosis was also confirmed by decreased pro-caspase 3 and increased PARP cleavage following exposure to the combination as measured by immunoblot (Figure 2E). In addition, as compared to single agent treatment, the level of p21 was increased after exposure to GSK126 and romidepsin (Figure 2E).

Co-exposure to GSK126 and romidepsin leads to enhanced acetylation and hypomethylation of H3K27 as well as dissociation of the PRC2 complex

To understand the effects of dual epigenetic targeting on both acetylation and methylation of histone, 4 GC-DLBCL cell lines were exposed to control, GSK126, romidepsin or the combination. Treatment with GSK126 and romidepsin led to increased acetylation and decreased tri-methylation of H3K27 as compared to single agents as detected by histone extraction and immunoblot (Figure 3A). These findings were validated by mass spectrometry (Figure 3B-E).

Protein levels of EZH2 and other members of PRC2 complex (SUZ12, EED, RbAp 46/48) were significantly decreased after dual treatment with GSK126 and romidepsin compared to single agent exposure (Figure 3F). Co-immunoprecipitation pull-down with EZH2 demonstrated dissociation of the PRC2 complex after simultaneous exposure to GSK126 and romidepsin. Specifically, exposure to romidepsin alone or in combination with GSK126 led to dissociation of EZH2 from EED, RbAp 46/48 and AEBP2 as compared to control, suggesting that romidepsin directly contributes to the breakdown of the PRC2 complex (Figure 3G). In addition, HDAC2 and DNMT3L were also found to disassemble from the EZH2-PRC2 complex after

combination therapy. Mass spectrometry confirmed disappearance of members of the PRC2 complex from EZH2 (Figure 3H-I). With this in mind, we hypothesized that romidepsin may be responsible for the disruption of the PRC2 complex through direct acetylation of one or more subunits of the complex. To evaluate this hypothesis, SU-DHL-10 cells were treated with romidepsin and immunoprecipitation using acetyl-lysine antibodies was performed. Based on mass spectrometry analysis, a 2-fold increase estimated by spectral counts of RbAp 46/48 (RBBP4) was observed after exposure to romidepsin as compared to control (FDR < 1.0%) (Figure 3J). Taken together, this suggests that the disruption of the PRC2 complex was secondary to direct acetylation of RbAp 46/48, which is responsible for PRC2 complex recruitment to nucleosomes [41].

HDAC2 plays a critical role in the synergy between GSK126 and romidepsin

Based on the finding that HDAC2 dissociated from PRC2 complex after dual inhibition of EZH2 and HDACs (Figure 3G), direct targeting of HDAC2 using a selective HDAC 1/2 inhibitor, ACY957[42], was combined with GSK126 and was found to be synergistic (Figure 4B). HDAC2 short hairpin RNA (shRNA) constructs were developed in order to confirm the role of HDAC2 inhibition in the synergy between GSK126 and romidepsin. Increased acetylation of H3K27 was found in HDAC shRNA HEK 293T cells, mimicking the effects of romidepsin, which was further enhanced by treatment with GSK126 (Figure 4C). Decreased methylation of H3K27 was more pronounced in HDAC2 shRNA cells treated with GSK126, mirroring the effects of GSK126 and romidepsin exposure. Single agent GSK126 exposure in HEK 293T cells did not significantly change the status of acetylation or methylation of H3K27.

GSK126 and romidepsin leads to improved overall survival and tumor growth delay in an in vivo mouse xenograft model

A SU-DHL-10 mouse xenograft model was selected due to the fact that SU-DHL-10 represents a GC-DLBCL cell line that harbors an EZH2 activating mutation as well as HAT mutations (CREBBP and EP300). Mice were exposed to control, GSK126, romidepsin, or the combination as detailed in Figure 5A. The combination

was well tolerated in mice with no appreciable change in weight (Figure 5B). Compared to single agent exposure, dual therapy with GSK126 and romidepsin led to significant tumor growth delay ($p < 0.05$), and increase overall survival ($p<0.0001$) (Figures 5C, D). Moreover, pre-treatment with GSK126 for 1 week did not improve tumor growth kinetics as compared to simultaneous exposure (Supplementary Fig. S2C, D).

Pharmacokinetic analysis of both serum and tumor samples were performed after a single exposure to GSK126 and romidepsin at various time points. The median Cmax of GSK126 was 1657.5 +/- 413.6 ng/mL which translates to 3.15 µM (in vitro IC_{50} of GSK126 in SU-DHL-10 is 0.7 µM), while romidepsin was 98.24 +/- 62.50 ng/mL or 0.18 µM (in vitro IC_{50} of romidepsin in SU-DHL-10 is 2.59 nM) (Figure 5E, F). The serum $AUC_{0\text{-last}}$ of GSK126 and romidepsin were 2828.57 (h*ng/mL), and 5.51(h*ng/mL), respectively. The intratumor concentration of GSK126 increased over time, while the romidepsin concentration was below the level of detection. A similar observation was observed in prior work performed by our group during which the intratumor levels of alisertib increased over time, while intratumor levels of romidepsin were below the level of detection after combination therapy[25].

Synergistic cell lines share a common basal gene expression and protein activity profile

Differential gene expression profiling was performed on pre-treatment lymphoma cell lines to determine their basal expression pattern and correlated to synergy (n=21). Cell lines with EOB ≥ 20 after treatment with GSK126 and romidepsin were defined as synergistic. There was a total of 69 genes identified (FDR <0.2) that were differentially expressed in the synergistic cell lines compared to non-synergistic cell lines, suggesting that a common basal gene expression profile is shared amongst the synergistic cell lines (Figure 6A, Supplementary Fig. S5). Pathway analysis determined by GSEA revealed synergistic cell lines are characterized by upregulation in chromatin remodeling genes and transcriptional regulators such as HDAC9 and HCFC1 as well as pathways implicated in epigenetic regulation (Figure 6 A, B). Moreover, of the 69 genes that were found to be differentially expressed in synergistic cell lines compared to non-synergistic cell lines, 34 genes have been

identified to be altered in more than 1.0% of primary patient DLBCL samples as confirmed by TCGA database and cBioPortal (Supplementary Fig. S6)[18].

metaVIPER was used to identify proteins whose activity predicts, and potentially mediates, sensitivity to dual EZH2-HDAC inhibition in lymphoma cell lines. We computed a differential protein activity signature between cell lines that demonstrate synergy by EOB and those that did not, and subsequently performed pathway analysis on this signature. Synergistic cell lines were markedly enriched in pathways involving cell cycle control, DNA replication, and chromatin remodeling (Figure 6C). This finding is similar to what was observed using GSEA at the RNA expression level. Downregulated pathways include inflammatory pathways as well as differentiation/developmental genes (Figure 6D).

Differential protein activity on 48 TCGA DLBCL primary patient samples was inferred using a pan-TCGA reference to compute gene expression signatures followed by interrogation with metaVIPER. Eighty-one percent of DLBCL tumors demonstrate significantly increased EZH2 activity (Bonferroni p-value < 0.01), in spite of only a few of the tumors harboring mutations in EZH2. Unbiased co-segregation analysis between EZH2 and a set of 400 'druggable' proteins demonstrated that the aberrant activity of several proteins are strongly associated with EZH2 activation, including HDAC 1/2 and DNMT (Figure 6E), further supporting dual targeting of EZH2 and HDACs in DLBCL. Taken together, interrogation of protein activity as a means to identify essential pathways that are common among synergistic cell lines describe a cellular state that is characterized by a (1) high level of proliferation; (2) transcriptional silencing through chromatin remodeling/condensation; (3) halt in cellular differentiation; and lastly; (4) suppression of inflammatory response. Interestingly, TGFβ signaling, which promotes T-regulatory cell function, is found to be more enriched in non-synergistic cell lines.

Many groups have demonstrated that gene expression profiles can be used to develop robust classifiers to predict drug sensitivity, but are difficult to validate in new datasets due to the inherent noise of RNA expression measurements and the risk of false discovery [33]. In contrast, VIPER inference of protein activity is highly reproducible and biologically relevant. We developed a random forest classifier from the basal protein activity profiles of this diverse set of lymphoma cell lines to predict synergy between GSK126 and romidepsin. This classifier demonstrated good receiver operating characteristics on 3-fold cross validation, with an AUC of 0.89 and an accuracy rate of 0.83 for predicting synergy (Supplementary Fig. S7). The classifier plateaued in performance with the inclusion of only 8 proteins (NDUFA13, CREBRF, MRPL12, KAT2B, ASF1B, BMPR2, POLRSI, IL65T), consistent with the ability of VIPER to identify biologically relevant proteins. Interestingly, decreased activity of KAT2B, an important HAT protein, was one of the most prominent features in the classifier for predicting synergistic activity of GSK126 and romidepsin.

DISCUSSION

Epigenetic alterations have been implicated as drivers of lymphomagenesis, with EZH2 dysregulation and HAT inactivating mutations being central to the pathogenesis of GC-DLBCL. Given the prominence of EZH2 dysregulation in lymphoma, selective EZH2 inhibitors have been developed and have shown single-agent activity in early clinical studies[13,43]. Individually, mutations in EZH2 and HAT produce a repressed transcriptional state, and together, the PRC2 complex recruits HDAC 1/2 leading to additional transcriptional repression. In this context, dual inhibition of EZH2 and HDACs may serve as a rational therapeutic platform in lymphomas harboring epigenetic derangements (Figure 2A). We describe that the combination of GSK126 and romidepsin was synergistic in EZH2 dysregulated lymphoma cell lines secondary to disassembly of the PRC2 complex due to acetylation of RbAP 46/48. This in turn caused attenuation of H3K27 methylation, increased acetylation, upregulation of p21, which together triggered apoptosis.

Acetylation of tumor suppressors and oncogenes have been well described[16,44]. EZH2 has been shown to be directly acetylated by P300/CBP-associated factor (PCAF) and deacetylated by SIRT1 in lung adenocarcinoma models, with acetylation of EZH2 having no effects on EZH2's ability to interact with other members of the PRC2 complex[45]. Acetylation of EZH2 itself was not identified in our studies, however, we demonstrate that exposure to GSK126 and romidepsin leads to acetylation of RbAP 46/48, in turn, causing instability of the PRC2 complex, preventing EZH2 from catalyzing trimethylation, leading to an open chromatin state.

Xenograft experiments demonstrated improvement in overall survival and tumor growth delay favoring the combination arm. Interestingly, intra-tumor concentrations of romidepsin were below the level of detection after co-treatment with GSK126 and romidepsin, which we have observed in prior combination studies[25]. However, despite the undetectable intratumor concentration of romidepsin, intratumor concentrations of GSK126 increased over time, with the combination arm demonstrating potent synergy compared to single agent therapy as manifested by increased overall survival and delayed tumor growth kinetics. Although complete tumor shrinkage was not observed in our xenograft studies, SU-DHL-10 has a very high proliferative rate owing to the fact that it harbors translocations of both MYC and BCL2 classifying it as a double hit lymphoma[46]. Double hit lymphomas are most frequently of germinal center origin and are notoriously clinically challenging as patients often relapse after first-line therapy and salvage chemotherapy[47]. Thus, our data may suggest a role of dual inhibition of EZH2 and HDACs for the treatment of double hit lymphomas. Given there has been limited success in identifying targeted therapy for double hit lymphomas this warrants further investigation.

With the use of next-generation sequencing, individualized approaches to cancer therapy may arise based on unique gene expression patterns and mutational profiles that collectively contribute to a specific molecular phenotype. In an effort to identify a gene expression profile that may select patients that would benefit from dual EZH2 and HDAC inhibition, pre-treatment RNA sequencing on a panel of lymphoma cell lines was performed. Cell lines demonstrating synergy to combined epigenetic therapy share a common basal genetic

signature with enrichment in chromatin remodeling and gene silencing pathways, with identification of 69 genes that are expressed in a similar pattern. Using metaVIPER, enrichment of chromatin modification and epigenetic pathways were verified, but it also identified enrichment of DNA repair/synthesis and cell cycle regulation pathways as well as down regulation of immune/inflammatory pathways in synergistic cell lines as compared to non-synergistic cell lines. Interestingly, recent evidence suggests that EZH2 and DNMT1 inhibit tumor cell production of T helper 1 type cytokines CXCL9 and CXCL10 as well as infiltration by effector T-cells, all of which can be reversed by inhibition of EZH2 and DNMT[48]. Correlative studies to characterize the tumor T-cell infiltrate in the context of pre- and on-treatment biopsies after treatment with EZH2 inhibitor in conjunction with HDAC inhibitor would further assist in understanding these observations. Therefore, a phase I/II clinical trial investigating this novel combination with extensive biological correlatives is in development.

In line with the shift towards precision medicine, recent genomic analysis of primary DLBCL patient samples has led to 2 new proposed DLBCL classification systems, including an 'EZB signature' characterized by EZH2 mutations and BCL2 translocations[49], and a 'cluster 3' subgroup identified by BCL2 mutations in conjunction with KMT2D, CREBBP, and EZH2 dysregluation[50] . The identification of a DLBCL molecular subtype, predominately of GC-origin, characterized by EZH2 mutations and BCL2 abnormalities in conjunction with the data presented here suggests that the addition of a BCL2 inhibitor to the combined inhibition of EZH2 and HDACs may be synergistic. This ultimately requires further investigation.

Our findings provide the biologic rationale and lay the groundwork for a future clinical trial of targeted epigenetic therapy in GC-DLBCL. The combination of dual EZH2 and HDAC inhibition may potentially serve as a precision medicine therapeutic platform in lymphomas derived from the GC and those harboring an epigenetically repressed transcriptional state.

ACKNOWLEDGEMENTS

This work was supported by the American Society of Clinical Oncology (ASCO) Young Investigator Award (JKL), SWOG HOPE Foundation SEED Fund (JEA), the National Resource for Translational and Developmental Proteomics under Grant P41 GM108569 from the National Institute of General Medical Sciences, National Institutes of Health (NLK), the Sherman Fairchild Foundation (NLK), and the Proteomics Shared Resource of the Herbert Irving Comprehensive Cancer Center/Columbia University Irving Medical Center (P30CA013696). We would like to also acknowledge the Lymphoma Research Fund of Columbia University for its generous support.

AUTHOR CONTRIBUTIONS

JKL and JEA wrote the manuscript. JEA, JKL, and SAP devise the experiments. JKL, JEA, SAP and YL interpreted the experimental results. JKL and SAP equally contributed to experiments. JKL performed cell viability, drug combinations, in vivo mouse studies and Non-compartmental analysis of PK/PD results. SAP performed western blots, co-immunoprecipitations, flow cytometry and HDAC shRNA. YL, YG and SM assisted in HDAC shRNA experiments. AV and OE performed RNA sequencing analysis. NA, NLK and JMC performed mass spectrometry for H3K27 modification. EC performed mass spectrometry for acetylation of PRC2 complex. CQ, RN, and SC performed PK/PD. PSM performed metaVIPER.

REFERENCES

1. Bracken AP, Helin K. Polycomb group proteins: navigators of lineage pathways led astray in cancer. Nat Rev Cancer 2009;9:773-84.
2. Vire E, Brenner C, Deplus R, et al. The Polycomb group protein EZH2 directly controls DNA methylation. Nature 2006;439:871-4.
3. van der Vlag J, Otte AP. Transcriptional repression mediated by the human polycomb-group protein EED involves histone deacetylation. Nature genetics 1999;23:474-8.
4. Morin RD, Johnson NA, Severson TM, et al. Somatic mutations altering EZH2 (Tyr641) in follicular and diffuse large B-cell lymphomas of germinal-center origin. Nature genetics 2010;42:181-5.
5. Bodor C, O'Riain C, Wrench D, et al. EZH2 Y641 mutations in follicular lymphoma. Leukemia 2011;25:726-9.
6. Zhang X, Chen X, Lin J, et al. Myc represses miR-15a/miR-16-1 expression through recruitment of HDAC3 in mantle cell and other non-Hodgkin B-cell lymphomas. Oncogene 2012;31:3002-8.
7. Ntziachristos P, Tsirigos A, Van Vlierberghe P, et al. Genetic inactivation of the polycomb repressive complex 2 in T cell acute lymphoblastic leukemia. Nature medicine 2012;18:298-301.
8. Fujikawa D, Nakagawa S, Hori M, et al. Polycomb-dependent epigenetic landscape in adult T-cell leukemia. Blood 2016;127:1790-802.
9. Yang XP, Jiang K, Hirahara K, et al. EZH2 is crucial for both differentiation of regulatory T cells and T effector cell expansion. Sci Rep 2015;5:10643.
10. Knutson SK, Kawano S, Minoshima Y, et al. Selective inhibition of EZH2 by EPZ-6438 leads to potent antitumor activity in EZH2-mutant non-Hodgkin lymphoma. Molecular cancer therapeutics 2014;13:842-54.
11. McCabe MT, Ott HM, Ganji G, et al. EZH2 inhibition as a therapeutic strategy for lymphoma with EZH2-activating mutations. Nature 2012;492:108-12.
12. McCabe MT, Graves AP, Ganji G, et al. Mutation of A677 in histone methyltransferase EZH2 in human B-cell lymphoma promotes hypertrimethylation of histone H3 on lysine 27 (H3K27). Proceedings of the National Academy of Sciences of the United States of America 2012;109:2989-94.
13. Italiano A, Soria J-C, Toulmonde M, et al. Tazemetostat, an EZH2 inhibitor, in relapsed or refractory B-cell non-Hodgkin lymphoma and advanced solid tumours: a first-in-human, open-label, phase 1 study. The Lancet Oncology.
14. Pasqualucci L, Dominguez-Sola D, Chiarenza A, et al. Inactivating mutations of acetyltransferase genes in B-cell lymphoma. Nature 2011;471:189-95.
15. Andersen CL, Asmar F, Klausen T, Hasselbalch H, Gronbaek K. Somatic mutations of the CREBBP and EP300 genes affect response to histone deacetylase inhibition in malignant DLBCL clones. Leukemia research reports 2012;2:1-3.
16. Amengual JE, Clark-Garvey S, Kalac M, et al. Sirtuin and pan-class I/II deacetylase (DAC) inhibition is synergistic in preclinical models and clinical studies of lymphoma. Blood 2013;122:2104-13.
17. Kalac M, Scotto L, Marchi E, et al. HDAC inhibitors and decitabine are highly synergistic and associated with unique gene-expression and epigenetic profiles in models of DLBCL. Blood 2011;118:5506-16.
18. Gao J, Aksoy BA, Dogrusoz U, et al. Integrative analysis of complex cancer genomics and clinical profiles using the cBioPortal. Science signaling 2013;6:pl1.
19. Cerami E, Gao J, Dogrusoz U, et al. The cBio cancer genomics portal: an open platform for exploring multidimensional cancer genomics data. Cancer discovery 2012;2:401-4.
20. Borisy AA, Elliott PJ, Hurst NW, et al. Systematic discovery of multicomponent therapeutics. Proceedings of the National Academy of Sciences of the United States of America 2003;100:7977-82.
21. Berenbaum MC. Criteria for analyzing interactions between biologically active agents. Advances in cancer research 1981;35:269-335.
22. Garcia BA, Mollah S, Ueberheide BM, et al. Chemical derivatization of histones for facilitated analysis by mass spectrometry. Nature protocols 2007;2:933-8.
23. Zheng Y, Sweet SM, Popovic R, et al. Total kinetic analysis reveals how combinatorial methylation patterns are established on lysines 27 and 36 of histone H3. Proceedings of the National Academy of Sciences of the United States of America 2012;109:13549-54.
24. MacLean B, Tomazela DM, Shulman N, et al. Skyline: an open source document editor for creating and analyzing targeted proteomics experiments. Bioinformatics 2010;26:966-8.

25. Zullo K, Scotto L, Amengual JE, O'Connor OA. The Aurora A Kinase Inhibitor, Alisertib, Has Broad Activity In Nonclinical Models Of T-Cell Lymphoma and Is Highly Synergistic With Romidepsin, But Not With Pralatrexate Or The Proteasome Inhibitor, Ixazomib2013.
26. Jain S, Jirau-Serrano X, Zullo KM, et al. Preclinical Pharmacologic Evaluation of Pralatrexate and Romidepsin Confirms Potent Synergy of the Combination in a Murine Model of Human T-cell Lymphoma. Clinical cancer research : an official journal of the American Association for Cancer Research 2015.
27. Guidance for industry: Bioanalytical method validation. In: Administration FaD, ed. Maryland: FDA; 2013:34.
28. Dobin A, Davis CA, Schlesinger F, et al. STAR: ultrafast universal RNA-seq aligner. Bioinformatics (Oxford, England) 2013;29:15-21.
29. Trapnell C, Roberts A, Goff L, et al. Differential gene and transcript expression analysis of RNA-seq experiments with TopHat and Cufflinks. Nature protocols 2012;7:562-78.
30. Anders S, Pyl PT, Huber W. HTSeq--a Python framework to work with high-throughput sequencing data. Bioinformatics (Oxford, England) 2015;31:166-9.
31. Ritchie ME, Phipson B, Wu D, et al. limma powers differential expression analyses for RNA-sequencing and microarray studies. Nucleic acids research 2015;43:e47.
32. Chen JC, Alvarez MJ, Talos F, et al. Identification of Causal Genetic Drivers of Human Disease through Systems-Level Analysis of Regulatory Networks. Cell 2016;166:1055.
33. Shen Y, Alvarez MJ, Bisikirska B, et al. Systematic, network-based characterization of therapeutic target inhibitors. PLoS computational biology 2017;13:e1005599.
34. Ding H, Douglass EF, Jr., Sonabend AM, et al. Quantitative assessment of protein activity in orphan tissues and single cells using the metaVIPER algorithm. Nat Commun 2018;9:1471.
35. Basso K, Margolin Aa, Stolovitzky G, Klein U, Dalla-Favera R, Califano A. Reverse engineering of regulatory networks in human B cells. Nature genetics 2005;37:382-90.
36. aracne.networks: ARACNe-inferred gene networks from TCGA tumor datasets. R package version 1.4.0. 2017.
37. Love MI, Huber W, Anders S. Moderated estimation of fold change and dispersion for RNA-seq data with DESeq2. Genome Biol 2014;15:550.
38. Ding BB, Yu JJ, Yu RY, et al. Constitutively activated STAT3 promotes cell proliferation and survival in the activated B-cell subtype of diffuse large B-cell lymphomas. Blood 2008;111:1515-23.
39. analysis VIoP-abER. 2016.
40. Liberzon A. A description of the Molecular Signatures Database (MSigDB) Web site. Methods Mol Biol 2014;1150:153-60.
41. Nekrasov M, Wild B, Muller J. Nucleosome binding and histone methyltransferase activity of Drosophila PRC2. EMBO reports 2005;6:348-53.
42. Min C, Moore N, Shearstone JR, et al. Selective Inhibitors of Histone Deacetylases 1 and 2 Synergize with Azacitidine in Acute Myeloid Leukemia. PloS one 2017;12:e0169128.
43. Harb W, Abramson J, Lunning M, et al. 42OA phase 1 study of CPI-1205, a small molecule inhibitor of EZH2, preliminary safety in patients with B-cell lymphomas. Annals of Oncology 2018;29:mdy048.01-mdy.01.
44. Bereshchenko OR, Gu W, Dalla-Favera R. Acetylation inactivates the transcriptional repressor BCL6. Nature genetics 2002;32:606-13.
45. Wan J, Zhan J, Li S, et al. PCAF-primed EZH2 acetylation regulates its stability and promotes lung adenocarcinoma progression. Nucleic acids research 2015;43:3591-604.
46. Drexler HG, Eberth S, Nagel S, MacLeod RA. Malignant hematopoietic cell lines: in vitro models for double-hit B-cell lymphomas. Leukemia & lymphoma 2016;57:1015-20.
47. Landsburg DJ, Falkiewicz MK, Maly J, et al. Outcomes of Patients With Double-Hit Lymphoma Who Achieve First Complete Remission. J Clin Oncol 2017:Jco2017722157.
48. Peng D, Kryczek I, Nagarsheth N, et al. Epigenetic silencing of TH1-type chemokines shapes tumour immunity and immunotherapy. Nature 2015;527:249-53.
49. Schmitz R, Wright GW, Huang DW, et al. Genetics and Pathogenesis of Diffuse Large B-Cell Lymphoma. N Engl J Med 2018;378:1396-407.
50. Chapuy B, Stewart C, Dunford AJ, et al. Molecular subtypes of diffuse large B cell lymphoma are associated with distinct pathogenic mechanisms and outcomes. Nature medicine 2018;24:679-90.

Figure 1: Sensitivity to GSK126 is Predicted by the Presence of EZH2 Mutation
(A) Single agent GSK126 cell viability curves of 21 lymphoma cell lines (Blue=GC-DLBCL, Red=ABC-DLBCL, Green=T cell lymphoma, Black = Mantle cell lymphoma) after 144 hour exposure. (B) Cell viability curves for 21 lymphoma cell lines exposed to romidepsin at 72 hours. (C) IC50 values (144 hours) for respective cell lines after exposure to GSK126. Dysfunction is defined as overexpression (OE) of EZH2 and mutated EZH2 combined. (D) IC50 values after 72 hour exposure to romidepsin. There is a trend towards the presence of HAT mutation and sensitivity to romidepsin (p=0.05). Experiments were performed in triplicates and performed 3 times.

Figure 2: GSK126 and Romidepsin are Synergistic in EZH2 Dysregulated Lymphomas
(A) Given the frequency of EZH2 mutations along with HAT mutations, dual inhibition of these deregulated pathways may serve as a rational method to reverse transcriptional repressed state. (B) 72 hour co-exposure of GSK126 (G) and romidepsin (R) lead to potent synergy in lymphoma cell lines with EZH2 dysregulation as measured by Excess over Bliss (EOB). (C-D) G+R induces apoptosis in germinal center DLBCL cell lines at 48 hours as demonstrated by flow cytometry. (E) G+R leads to increase levels of p21, in turn, leading to apoptosis of 4 GC- lymphomas as depicted by cleavage of PARP and increased pro-Caspase-3 levels. Experiments were performed in triplicates and performed 3 times.

Figure 3: Combination of GSK126 and Romidepsin leads to Decreased Methylation and Increased Acetylation of H3K27 and Dissociation of the PRC2 complex
(A) Acetylation of H3K27 was increased after combination therapy as compared to single agent therapy. H3K27me3 decreased after the combination. (B-E) Mass Spectrometry confirms acetylation and methylation findings in 2 germinal center DLBCL cell lines. Fold change calculated relative to control. (F) Protein levels of EZH2 and PRC2 complex members are decreased after exposure to GSK126 and romidepsin as compared to single agent therapy. (G) Co-immunoprecipitation after treatment with GSK126, romidepsin or the combination demonstrates dissociation of the PRC2 complex members after exposure to the combination of GSK126 and romidepsin. (H-I) Mass spectrometry after 24h exposure to romidepsin (2.5nM) in SU-DHL-10 cells demonstrates dissociation of EZH2-SUZ12 from the PRC2 complex. (J) Mass spectrometry after co-IP with acetyl lysine antibody demonstrated a 2-fold increase estimated by spectral counts between untreated SU-DHL-10 cells and romidepsin exposed cells. Using Proteome Discoverer 2.1, this acetylated protein was identified as RbAp 46/48 (RBBP4) (FDR <1.0%).

Figure 4: The cooperation of the PRC2 complex and HDAC2 is essential in the Synergistic Effects of GSK126 and Romidepsin
(A) Cell viability curves in 4 GC-DLBCL cell lines after exposure to ACY957 at 72 hours. (B) GSK126 and ACY957 are synergistic as demonstrated by EOB in 4 GC-DLBCL cell lines. (C) Acetylation of H3K27 is enhanced by exposure to GSK126 in HDAC2 shRNA HEK 293T cells while methylation levels are attenuated. Experiments were performed in triplicates and performed 3 times.

Figure 5: Combination of GSK126 and Romidepsin Improves Overall Survival in a Mouse Xenograft Model
(A) Treatment schema. Combination arm received GSK126 on days 1, 4, 8, 11, 15, 18; romidepsin dosed on days 1, 8, 15. (B) Combination of GSK126 and romidepsin is tolerable as demonstrated by stability of weight. (C) Co-exposure to GSK126 and romidepsin leads to improved tumor control compared to single agent GSK126 or romidepsin. (D) Combination of GSK126 and romidepsin leads to improved overall survival compared to single agent GSK126 or romidepsin. (E) PK/PD parameters after single intraperitoneal injection of GSK126 and romidepsin. Intratumor GSK126 continues to increase over time and is still present at 24 hours. (F) Serum romidepsin pharmacokinetic parameters after single injection of GSK and romidepsin over 24 hours.

Figure 6: Synergistic Cell Lines Share a Common Basal Gene and Protein Signature

(A) Synergistic (EOB ≥20) cell lines display a common basal gene expression signature, with upregulated genes such as HDAC9, AHCY, and MBD3. Genes are fully listed in supplementary Fig. S5. (B) Synergistic cell lines share enrichment in epigenetic pathways. (C, D) Using Meta-VIPER, synergistic cell lines are enriched in pathways involving cell cycle control, DNA replication, and chromatin remodeling with downregulation of differentiation and inflammatory pathways. (E) Unbiased interrogation of 400 proteins revealed co-segregation of several proteins with EZH2 including HDAC 1/2, DNMT3B, and MYC in primary patient samples (TCGA).

Figure 1

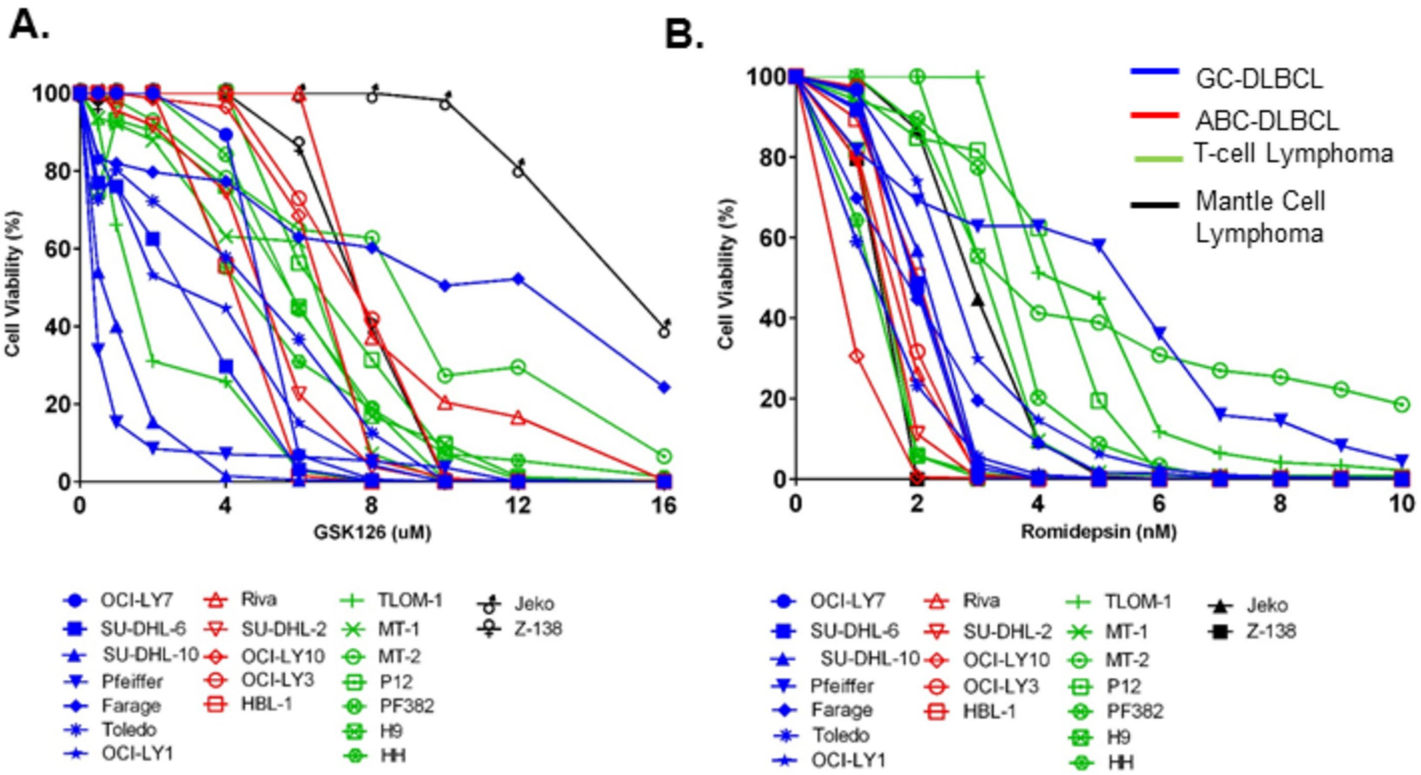

C.

Cell Lines	Subtype	EZH2 Status	IC50 GSK126 (μM)
Pfeiffer	GC-DLBCL	A677G	0.1
SU-DHL-10	GC-DLBCL	Y641F;Y646S	0.7
TLOM-1	ATLL	Overexpression	1.5
SU-DHL-6	GC-DLBCL	Y602N;Y646N	3.1
OCI-LY1	GC-DLBCL	Y602N;Y646N	3.7
HBL-1	ABC-DLBCL	Wildtype	4.2
OCI-LY7	GC-DLBCL	Wildtype	4.3
MT-1	ATLL	Overexpression	4.4
HH	CTCL	Wildtype	4.4
SU-DHL-2	ABC-DLBCL	Wildtype	4.9
PF-382	T-ALL	Wildtype	5.6
Toledo	GC-DLBCL	Wildtype	6
P12	T-ALL	Wildtype	6
H9	CTCL	Wildtype	6.1
OCI-LY10	ABC-DLBCL	Wildtype	6.4
Z-138	Mantle Cell	Overexpression	7.1
OCI-LY3	ABC-DLBCL	Wildtype	7.2
Riva	ABC-DLBCL	Wildtype	7.5
MT-2	ATLL	Overexpression	9
Jeko-1	Mantle Cell	Overexpression	10
Farage	GC-DLBCL	Wildtype	10

D.

Cell Lines	Lymphoma	EP300/CREBBP	IC50 Romidespin (nM)
OCI-LY10	ABC-DLBCL	EP300 non sen mut/CREBBP non ses mut	1.0
HBL-1	ABC-DLBCL	Wildtype	1.0
Toledo	GC-DLBCL	EP300 mis mut/CREBBP del	1.0
Z-138	Mantle Cell	Wildtype	1.1
Jeko-1	Mantle Cell	Wildtype	1.1
HH	CTCL	Wildtype	1.1
SU-DHL-2	ABC-DLBCL	Wildtype	1.3
H9	CTCL	Wildtype	1.3
Riva	ABC-DLBCL	Wildtype	1.5
OCI-LY7	GC-DLBCL	Wildtype	1.5
Farage	GC-DLBCL	EP300 fs / CREBBP mis mut	1.7
OCI-LY3	ABC-DLBCL	Wildtype	1.7
SU-DHL-6	GC-DLBCL	EP300 mis mut/CREBBP trunc mut	2.0
SU-DHL-10	GC-DLBCL	EP300 mis mut/CREBBP trunc mut	2.1
OCI-LY1	GC-DLBCL	CREBBP del	2.5
MT-2	ATLL	Wildtype	2.7
MT-1	ATLL	Wildtype	2.8
PF-382	T-ALL	CREBBP mis mut	3.5
TLOM-1	ATLL	Wildtype	4.3
P12	T-ALL	Wildtype	4.3
Pfeiffer	GC-DLBCL	CREBBP mis mut	6.0

	p-value
Dysfunction vs. WT	0.15
Mutated vs. WT	0.02
OE vs WT	0.52

	p-value
Mutated vs. WT	0.05

Figure 2

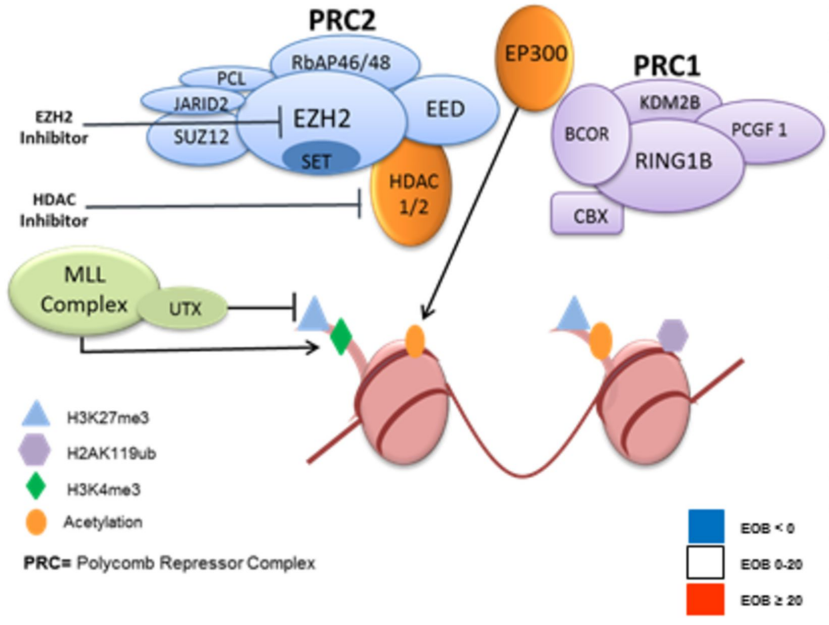

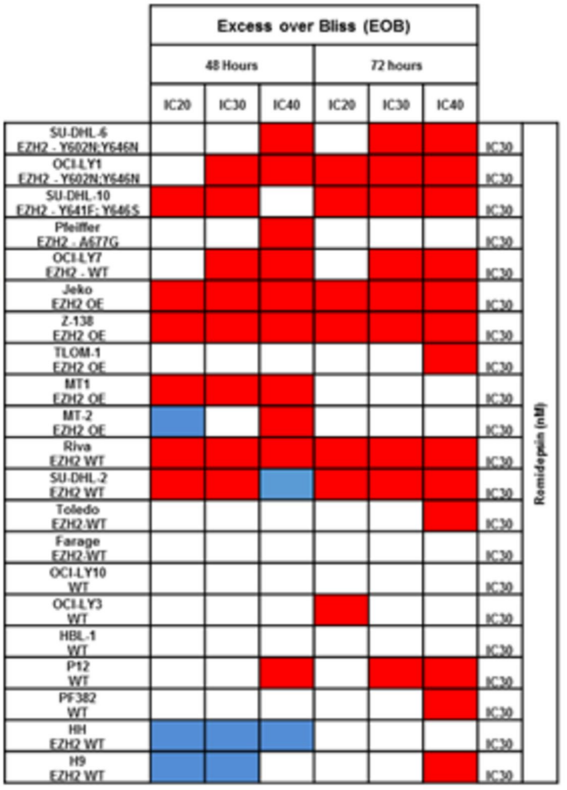

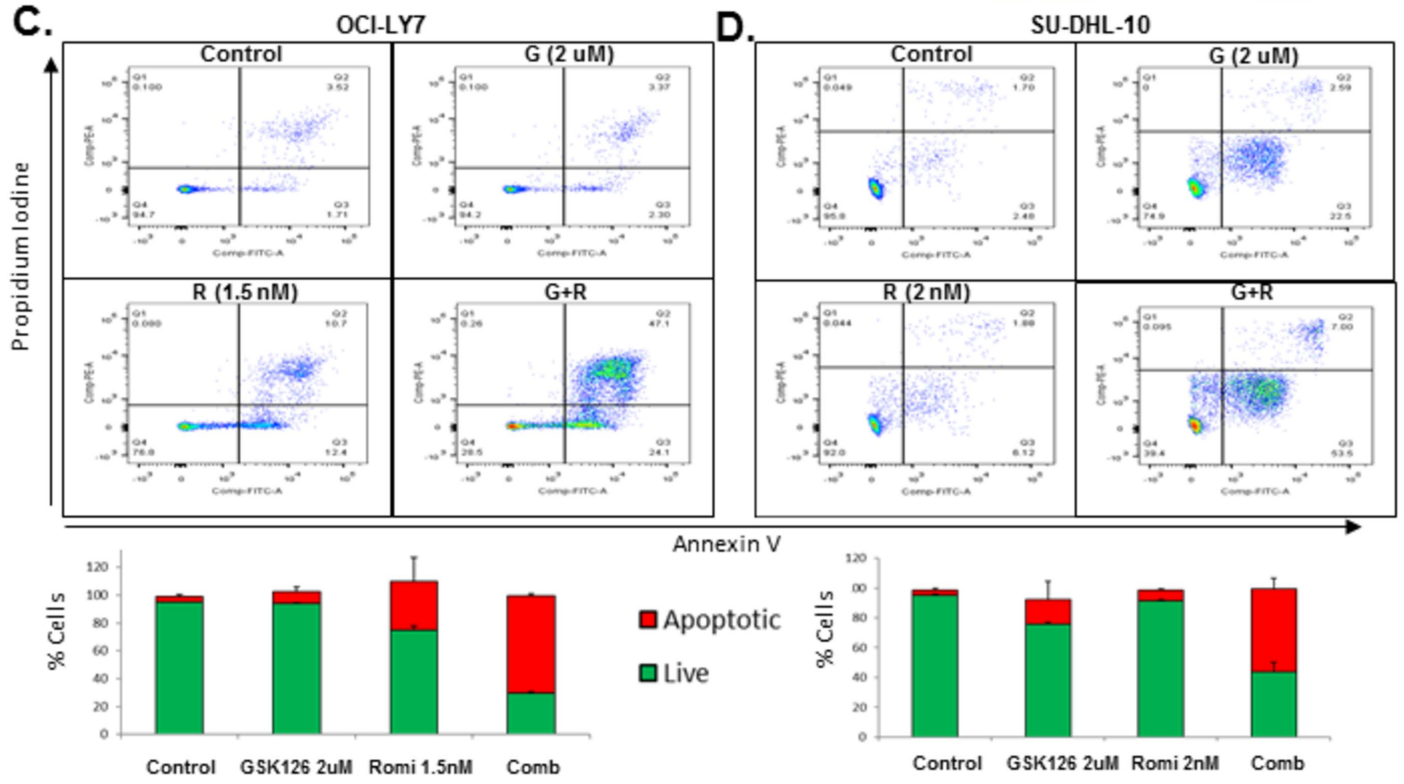

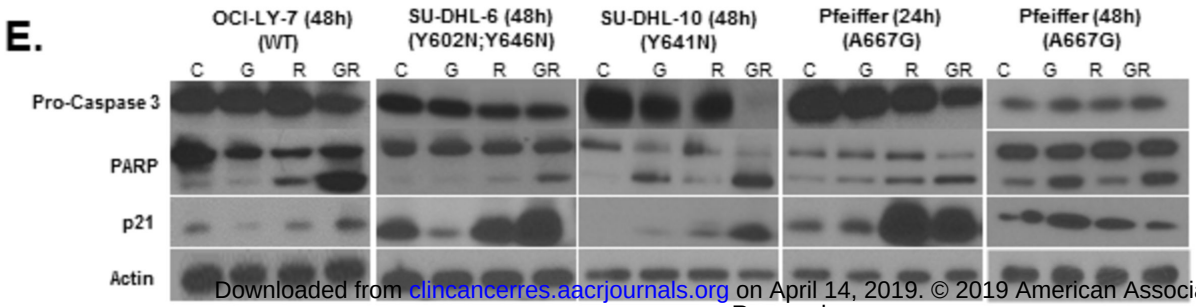

Figure 3

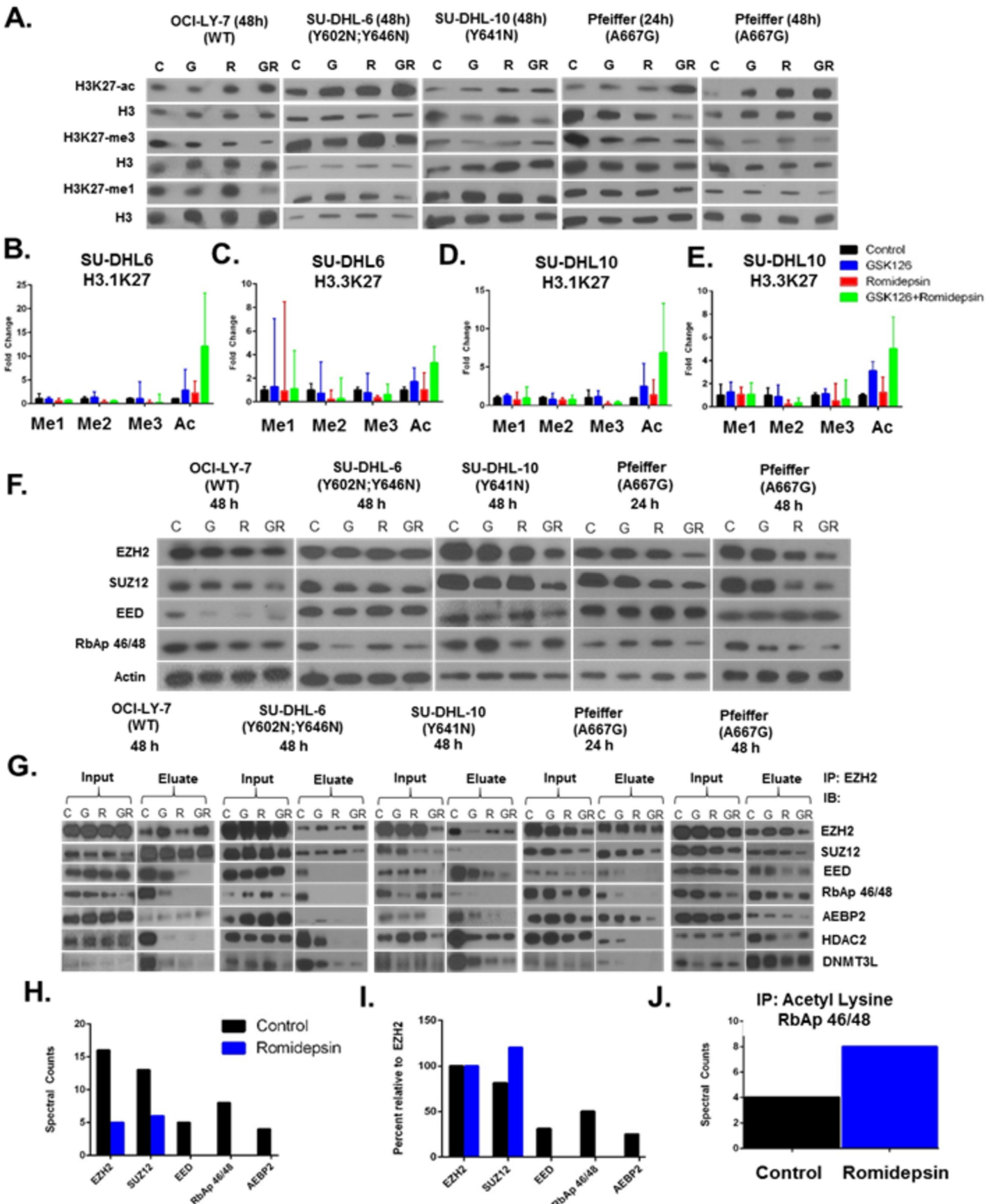

Figure 4

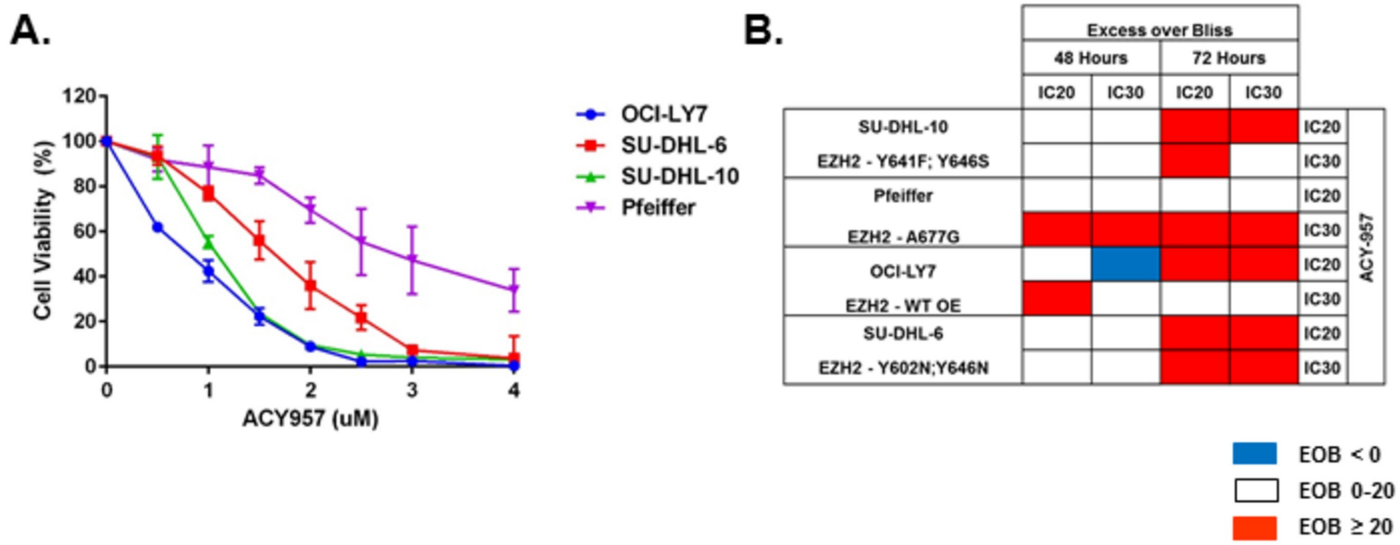

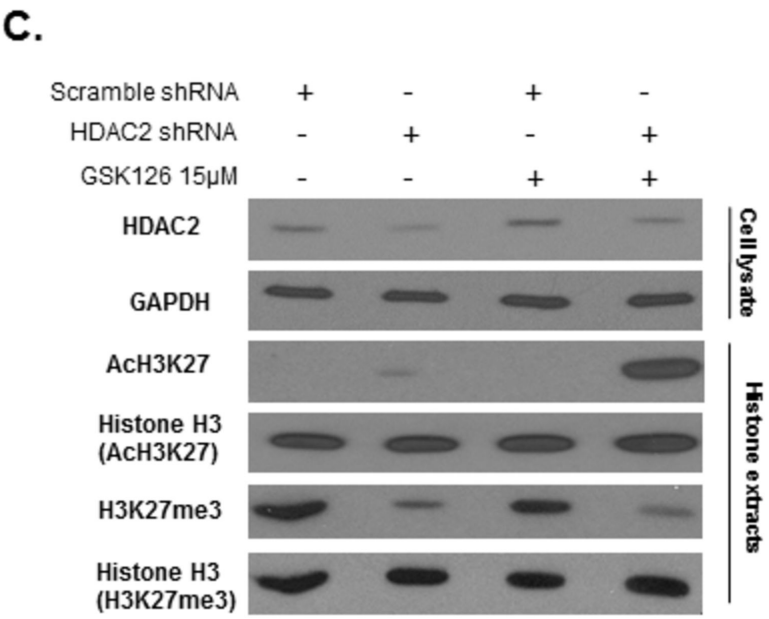

Figure 5

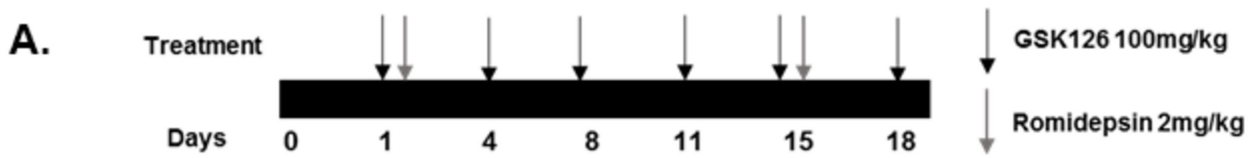

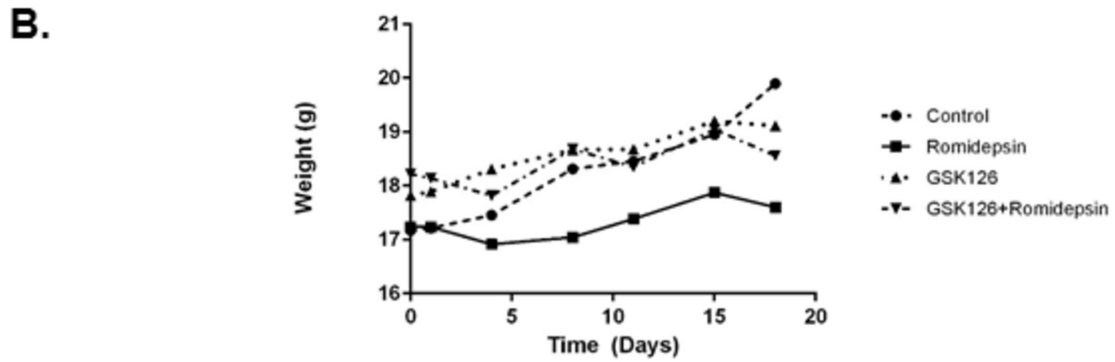

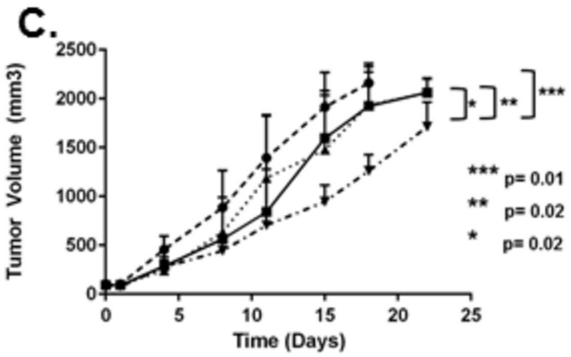

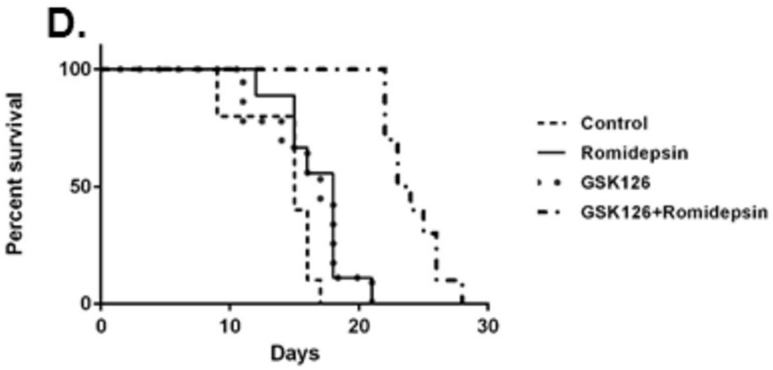

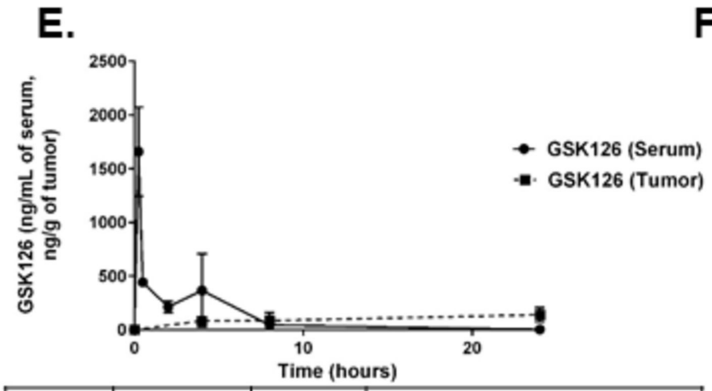

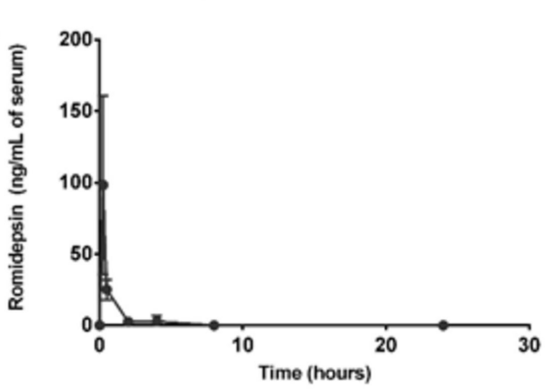

	AUC 0-last (h*ng/mL)	Tmax (hours)	Cmax (ng/mL of serum, ng/g of tumor)
Serum	2828.57	0.25	1657.54
Tumor	-	24	140.19

	AUC 0-last (h*ng/mL)	Tmax (hours)	Cmax (ng/mL of serum)
Serum	5.51	0.25	98.24

Figure 6

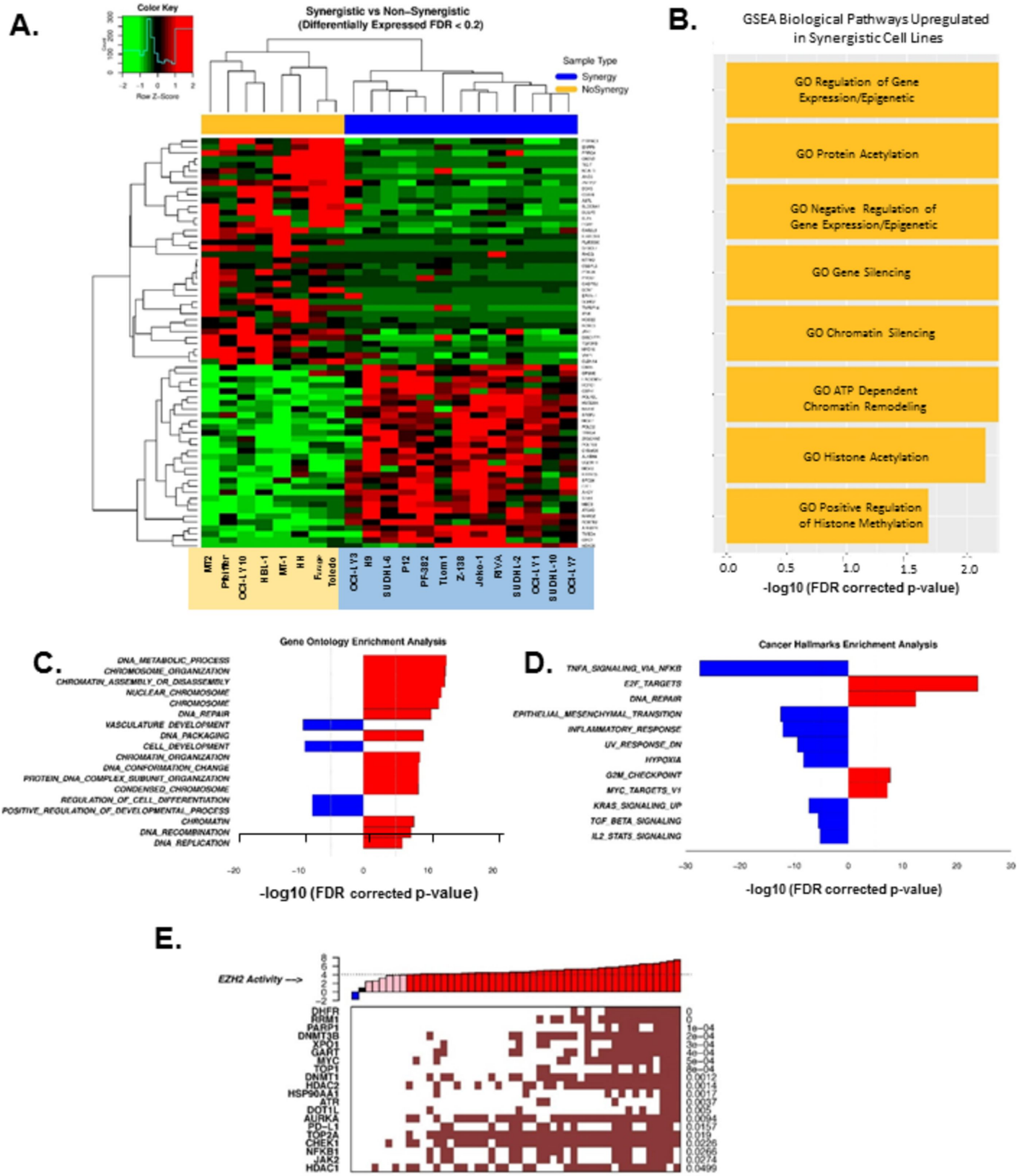

AACR American Association for Cancer Research

Clinical Cancer Research

Precision Targeting with EZH2 and HDAC Inhibitors in Epigenetically Dysregulated Lymphomas

Jennifer K Lue, Sathyen A Prabhu, Yuxuan Liu, et al.

Clin Cancer Res Published OnlineFirst April 12, 2019.